Current transformer saturation compensation based on a partial nonlinear model

D.Y. Shi [a], J. Buse [b], Q.H. Wu [b,a,*], C.X. Guo [c]

[a] School of Electric Power Engineering, South China University of Technology, Guangdong 510640, China
[b] Department of Electrical Engineering and Electronics, The University of Liverpool, Liverpool L69 3GJ, UK
[c] College of Electrical Engineering, Zhejiang University, Hangzhou 310027, China

A R T I C L E   I N F O

A B S T R A C T

This paper proposes a partial nonlinear model to accurately represent the nonlinear saturation characteristic of a current transformer (CT). Based on the model, the saturated section of the secondary current as well as the unsaturated section can be used in a regression process to estimate model parameters. The saturated section normally lies near the inception of a fault, therefore accurate parameters can be obtained faster compared with the methods using only unsaturated sections. The pre-fault remanent flux and DC-offset, which could significantly influence CT saturation, are both considered in the model, thus they do not affect the accuracy of the parameter estimation. The computational load of the regression calculation is significantly reduced by using separable nonlinear least squares (SNLLS) method. This provides the feasibility to implement the method for real-time protective relaying. The performance of the method has been evaluated on the data obtained from both PSCAD/EMTDC simulation and live recording with a test CT. The method has also been implemented in a Field Programmable Gate Array (FPGA).

1. Introduction

Iron-core current transformers (CTs) are widely used for current measurements in power systems due to their reliability and acceptable cost. Their major disadvantage is concerned with the saturation of the iron-cores, which causes the distortion of secondary currents appearing at the inputs of protection relays [1]. This may, in consequence, lead protection relays to malfunction. Two ways are normally used to alleviate this impact: (1) using large iron-core CTs to reduces the probability of the occurrence of CT saturation; (2) employing compensation algorithms to eliminate the influence of CT saturation. Obviously the latter is more economical.

In recent years, the techniques of compensating the secondary current distortion caused by CT saturation have been intensively studied. In [2], the magnetizing current of a saturated CT is estimated by applying the calculated instantaneous flux of the CT to the magnetization curve of the CT. This technique relies on the assumption that the remanent flux in the CT is zero prior to the fault, which has the drawback that the assumption cannot be guaranteed in every fault condition. In [3,4], the remanent flux problem is avoided by detecting the exact start points of the distorted secondary currents using difference functions and a morphological lifting scheme (MLS) respectively. The instantaneous flux at these

points is equal to the flux at the knee point in the magnetization curve of the CT. However, due to the disturbances caused by anti-aliasing filters and noise, the start points detected by these methods may have large deviations from their true values. Some methods use a complex inverse function to get the compensated current with the saturated current as input [5,6]. Usually, an artificial neural network (ANN) is used as the complex inverse function. Theoretically, ANN can provide satisfactory compensation. However, it has to be trained with comprehensive data, which cover all the possible saturation scenarios of the CTs. Without these data and sufficient training, the accuracy of the ANN approach would not be ensured. Another group of methods apply a linear regression [7] and a discrete dynamic filter [8] on the unsaturated sections of the secondary current to reconstruct the compensated current. They utilize wavelet and a threshold criteria respectively, to extract unsaturated sections from a distorted secondary current. Using these methods, sufficient length of unsaturated sections is required to obtain accurate results. If the methods are used to deal with a severely saturated current, which has only a very short unsaturated section in each fundamental cycle, more than one cycle of the current is needed to get enough unsaturated sections.

In [9] the authors has proposed a novel method which can compensate CT saturation current accurately and rapidly. In this paper, the method has been further developed, thoroughly verified and implemented in a Field Programmable Gate Array (FPGA) based embedded system. Based on a partial nonlinear model, both unsaturated and saturated sections of a distorted secondary current are used by the method to conduct a nonlinear regression, therefore only a short section of current waveform is required to achieve an

* Corresponding author at: Department of Electrical Engineering and Electronics, The University of Liverpool, Liverpool L69 3GJ, UK. Tel.: +44 1517944535; fax: +44 1517944540.
E-mail address: qhwu@liv.ac.uk (Q.H. Wu).

accurate estimation. Then a healthy secondary current waveform is reconstructed from the estimated parameters. The remanent flux is considered in the nonlinear part of the model, therefore it does not affect the accuracy of the estimated parameters. Tests show accurate parameters can be obtained within 0.5–0.8 of a cycle after fault occurrence. Moreover the phasor of the fault current could also be directly calculated from the parameters without waveform reconstruction. Normally, a multi-dimension nonlinear regression is difficult to be realized in a real-time embedded system, such as protection relays, due to its heavy computational load. However, this nonlinear regression can be transformed to a combination of a single dimension nonlinear regression and a multi-dimension linear regression by using separable nonlinear least squares (SNLLS) method. Thus, a great computational load reduction is achieved. The method has been implemented in an FPGA and tested in a real-time protection relay test bench. The test results indicate the potential of this method for future relaying applications.

2. Nonlinear regression model of secondary current

Fig. 1 presents a simplified equivalent circuit of a CT, where $i_p(t)$ is the primary current referred to the secondary side, $i_m(t)$ is the magnetizing current, $i_s(t)$ is the secondary current, Z_m is the excitation impedance, R_s and L_s are the total secondary resistance and inductance respectively. The relationship among the currents can be expressed as

$$i_p(t) = i_s(t) + i_m(t), \tag{1}$$

where $i_s(t)$ is measured through a CT. As functions of time, $i_p(t)$ and $i_m(t)$ are only rely on some undetermined constant parameters, thus (1) can be transformed to a regression model.

The primary fault current $i_p(t)$ is the superposition of a sinusoidal waveform (i.e., the phasor of the fault current) and an exponentially decaying DC-offset, which is determined by the factors: source voltage, circuit impedance, fault inception angle and X/R ratio of the primary fault path. It can be expressed as

$$i_p(t) = A\sin(\omega t + \theta) + Be^{-\tau t}, \tag{2}$$

where A is the amplitude, ω is the angular speed, and θ is the inception angle. B and τ are respectively the initial value and the time constant of the DC-offset. By respectively applying trigonometric expansion and first-order Taylor series expansion on the cosine term and the exponential term of the equation, a linear approximation can be obtained:

$$
\begin{aligned}
i_p(t) &= A\cos\theta\sin(\omega t) + A\sin\theta\cos(\omega t) + B - \tau t \\
&= a_1\sin(\omega t) + a_2\cos(\omega t) + a_3 + a_4 t,
\end{aligned} \tag{3}
$$

where $a_1 - a_4$ are unknown parameters.

The magnetizing current $i_m(t)$ is a function of CT core flux $\varphi(t)$. The function is also called the magnetization curve of the CT. It can be converted from the secondary-excitation curve of the CT provided by CT manufacturers. A high-order power series based
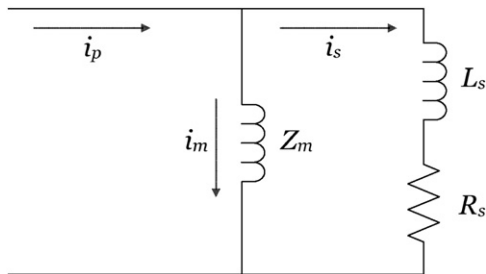

Fig. 1. Simplified equivalent circuit of a CT.

model introduced in [10] provides an accurate approximation to the curve. The typical expression of the model is

$$i_m(t) = k_1\varphi(t) + k_2\varphi(t)^5 + k_3\varphi(t)^{33}, \tag{4}$$

where $k_1 - k_3$ are the magnetizing characteristic of the CT. $\varphi(t)$ and $i_s(t)$ have a relationship described in

$$\frac{d\varphi(t)}{dt} = R_s i_s(t) + L_s \frac{di_s(t)}{dt}. \tag{5}$$

Integrating it from t_0 to t yields

$$\varphi(t) = R_s \int_{t_0}^{t} i_s(t)dt + L_s(i_s(t) - i_s(t_0)) + \varphi(t_0). \tag{6}$$

Substitute $\varphi(t)$ in (4) with (6) and set remanent flux $\varphi(t_0)$ as an unknown parameter a_5, $i_m(t)$ can be represented as a function F_{im}.

$$i_m(t) = F_{im}([i_s(t_0), i_s(t_1)\cdots i_s(t)], a_5), \tag{7}$$

where $[i_s(t_0), i_s(t_1)\cdots i_s(t)]$ denotes the samples of the secondary current between t_0 and t. Then a nonlinear regression model (8) is obtained by substituting (8) and (7) into (1).

$$
\begin{aligned}
i_s(t) &= a_1\sin(\omega t) + a_2\cos(\omega t) + a_3 + a_4 t \\
&\quad - F_{im}([i_s(t_0), i_s(t_1)\cdots i_s(t)], a_5).
\end{aligned} \tag{8}
$$

Inside, parameters $a_1 - a_5$ are unknown. The regression analysis based on this model aims to estimate $a_1 - a_5$ using the sampled secondary fault current.

3. SNLLS based regression scheme

A nonlinear regression function $\mathbf{f}_i(\mathbf{a})$ can be formed by shifting all the terms in (8) to the right side of the equation. This gives

$$
\begin{aligned}
\mathbf{f}_i(\mathbf{a}) &= i_s(t_i) + F_{im}([i_s(t_0)\cdots i_s(t_i)], a_5) - (a_1\sin(\omega t_i) + a_2\cos(\omega t_i) \\
&\quad + a_3 + a_4 t_i),
\end{aligned} \tag{9}
$$

where $\mathbf{a}$ is the vector of unknown parameters $a_1 - a_5$. Applying (9) to m samples of secondary fault current yields

$$\mathbf{f}(\mathbf{a}) = \mathbf{i_s} + \mathbf{F_{im}}(a_5) - \mathbf{La}_{(1-4)}, \tag{10}$$

where $\mathbf{f}(\mathbf{a}) = [\mathbf{f}_0(\mathbf{a})\,\mathbf{f}_1(\mathbf{a})\ldots\mathbf{f}_{m-1}(\mathbf{a})]^T$, $\mathbf{i_s} = [i_s(t_0)\,i_s(t_1)\ldots i_s(t_{m-1})]^T$, $\mathbf{F_{im}}(a_5) = [F_{im}([i_s(t_0)], a_5)\ldots F_{im}([i_s(t_0), i_s(t_1)\cdots i_s(t_i)], a_5)]^T$, $\mathbf{a}_{(1-4)} = [a_1\,a_2\,a_3\,a_4]^T$, and

$$
\mathbf{L} = \begin{bmatrix}
\sin(\omega t_0) & \cos(\omega t_0) & 1 & t_0 \\
\sin(\omega t_1) & \cos(\omega t_1) & 1 & t_1 \\
\vdots & \vdots & \vdots & \vdots \\
\sin(\omega t_{m-1}) & \cos(\omega t_{m-1}) & 1 & t_{m-1}
\end{bmatrix}.
$$

Then, the least squares problem of the regression model can be expressed in a matrix format as

$$r_{NLLS}(\mathbf{a}) = \mathbf{f}(\mathbf{a})^T\mathbf{f}(\mathbf{a}). \tag{11}$$

Nonlinear least squares (NLLS) problems do not have analytical form solutions and normally solved by iterative refinement. The computational load needed to solve a NLLS problem mainly depends on its convergence speed and the load of each iteration. The computational load needed to solve (11) can be greatly reduced by exploiting the partial nonlinear characteristic of (10). Inside, only a_5 relates to the nonlinear function $\mathbf{F_{im}}(a_5)$, and $\mathbf{a}_{(1-4)}$ have linear relationships with $\mathbf{L}$. By using SNLLS method [11], the 5-dimension NLLS problem, $r_{NLLS}(\mathbf{a})$, can be converted to a one-dimension NLLS problem and a 4-dimension LLS problem. First, (10) turns to a LLS
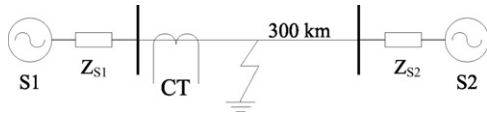
Fig. 2. Sample power system model.

problem by assuming a_5 is known. Accordingly, its analytical solution is

$$\mathbf{a}_{(1-4)} = \mathbf{L}^+(\mathbf{i_s} + \mathbf{F_{im}}(a_5)), \qquad (12)$$

where $\mathbf{L}^+$ is the Moore–Penrose generalized inverse of $\mathbf{L}$ and can be calculated by $\mathbf{L}^+ = (\mathbf{L^T L})^{-1}\mathbf{L}^T$. Then, by replacing $\mathbf{a}_{(1-4)}$ in (10) with (12), a one-dimension NLLS problem is formed as

$$r_{\text{SNLLS}}(a_5) = \mathbf{f}_{\text{SNLLS}}(a_5)^T \mathbf{f}_{\text{SNLLS}}(a_5), \qquad (13)$$

where

$$\mathbf{f}_{\text{SNLLS}}(a_5) = (\mathbf{I} - \mathbf{LL}^+)(\mathbf{i_s} + \mathbf{F_{im}}(a_5)). \qquad (14)$$

Once a_5 is obtained, $\mathbf{a}_{(1-4)}$ can be calculated by applying it back to (12). The amplitude and the relative phase of the fundamental waveform of the fault current can also be directly calculated from $\sqrt{a_1^2 + a_2^2}$ and $\arctan(a_2/a_1)$, respectively.

The NLLS problems described in (11) and (13) are solved by using two widely adopted NLLS solving methods, Powell's Dogleg trust-region method [12] and Levenberg–Marquardt (LM) method [13]. Test results have shown that the convergence speed of the two methods increases around by 50 percent when SNLLS method is applied, and generally Dogleg trust-region method performs better than LM method under the same conditions.

According to the analysis of the profile of the one-dimension objective function $r_{\text{SNLLS}}(a_5)$, which is shown in Fig. 3. It is a non-convex function. It is well understood that when solving non-convex functions, the performance of Quasi-Newton NLLS solvers (e.g., LM method, Dogleg method) is affected by the initial points of the iterations. To guarantee always finding the globe minimum of $r_{\text{SNLLS}}(a_5)$ (i.e. convergence), the initial points are set to be equal to positive or negative maximum possible core flux of the CT according to the polarity of the saturation. A simple MLS based method introduced in [4] is applied to determine the existence of CT saturation and its polarity.

4. Performance evaluation

To evaluate the performance of the proposed method, a wide range of test cases were established and analyzed. The test cases are divided into two groups with respect to the sources of test data: (a) the simulation data generated form PSCAD/EMTDC, and (b) the real data live recorded from a test CT. The real data are provided by courtesy of Siemens Protection Devices Ltd. In the following description, all of the quantities are referred to the secondary side. The sampling rate is 32 points per cycle. To measure the compensation accuracy
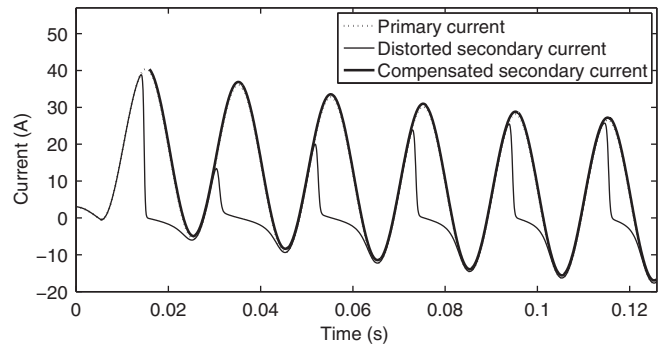

Fig. 4. Compensated result of case 1.

of the test cases in the following sections, a normalized root mean square error $\varepsilon_{\text{NRMS}}$ is defined as

$$\varepsilon_{\text{NRMS}}\% = \frac{\sqrt{(1/N)\sum_{n=1}^{N}(i_p(n) - i_{cs}(n))^2}}{\max(i_p) - \min(i_p)} \times 100, \qquad (15)$$

where i_{cs} is a compensated secondary current.

4.1. Test cases with simulation data

A sample power system model, as shown in Fig. 2, is built in PSCAD to generate test data. The model consists of two sources and a single transmission line. S1 and S2 are equivalent AC voltage sources whose phase-to-phase voltages are both 220 kV but with different phase angles. Z_{S1} and Z_{S2} are equivalent impedances of S1 and S2. The length of the transmission line is 300 km. Single phase to ground faults are put on the line. To cover all possible operation conditions, various parameters are used, including fault locations (10–150 km), fault inception angles (0–315°), X/R ratio (10–60) and fault resistance (0.1–5 Ω). The CT model used in the simulation is based on Jiles–Atherton theory [14]. Its settings are: ratio (1000:5), secondary resistance (0.5 Ω) and secondary inductance (0.8×10^{-3} H). A pure resistive or 0.5 power factor (pf) burden is connected to the secondary side. The remanent flux is set to be in the range of −80% to 80% of the saturation flux of the CT.

In total, 274 simulation data sets have been generated using the model. A consecutive window of a half cycle is applied in the compensation calculation. The average and maximum $\varepsilon_{\text{NRMS}}$ of these tests is 1.03% and 5.12%, respectively. To illustrate the performance of the proposed method, five representative test cases, which cover typical fault scenarios, are presented below. The configurations of these five cases are given in Table 1.

1) *Case 1: normal saturation scenario*

Case 1 represents a normal saturation scenario. Fig. 4 shows the compensated result. The bold line is the reconstructed secondary current, which is an accurate approximation of the primary current. It also shows that the valid output of the
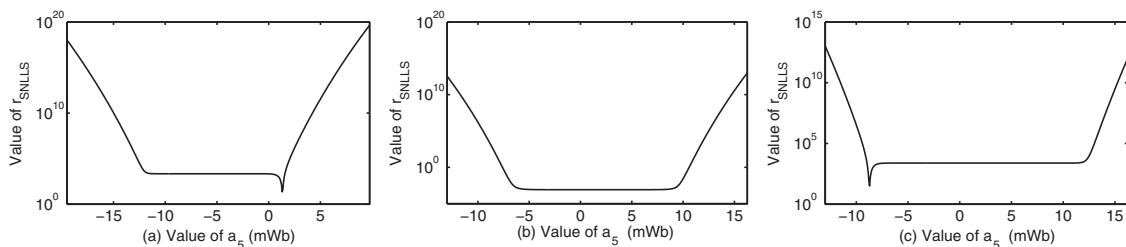

Fig. 3. Profiles of $r_{\text{SNLLS}}(a_5)$ under different condition. (a) Saturation with positive polarity and no remanent flux. (b) No saturation. (c) Saturation with negative polarity and −80% remanent flux (i.e., the remanent flux is 80% of the flux at the CT saturation point with negative polarity).

Table 1
Configurations of test cases 1–5.

	X/R ratio	Remanent flux	Fault inception angle	Fault location	Fault resistance	Secondary burden
Case 1	30	0%	0°	80 km	0.1 Ω	25 Ω
Case 2	40	80%	45°	100 km	0.1 Ω	25 Ω
Case 3	20	0%	180°	80 km	2 Ω	30 Ω, 0.5 pf
Case 4	60	80%	45°	10 km	0.1 Ω	1.5 Ω
Case 5	20	0%	90°	30 km	0.1 Ω	50 Ω
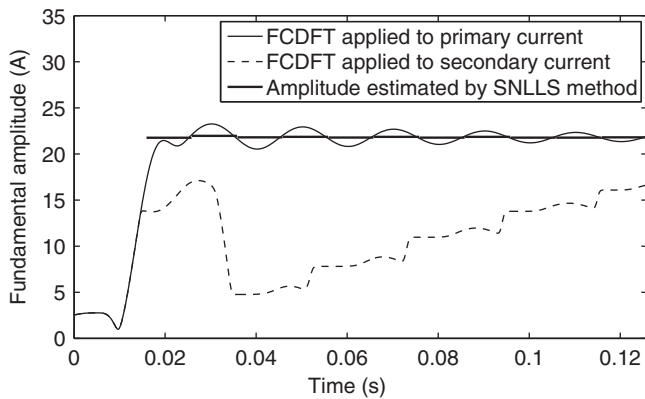
Fig. 5. Comparison of the values of fundamental amplitude of case 1.

method can be obtained within about 10 ms after the fault occurrence. The phasor calculated from a_1 and a_2 is given in Fig. 5. Inside it is compared with that obtained from full-cycle discrete Fourier transform (FCDFT). The value of ε_{NRMS} is 1.36%. In this case the Dogleg method and LM method need respectively 19 and 47 iterations to solve (11). After applying SNLLS, the iteration numbers reduces to 8 and 12 respectively, less than half of the original iteration numbers.

2) *Case 2: heavy remanent flux scenario*

The remanent flux has a great effect on the first half cycle of the secondary fault current. This case illustrates a severe saturation caused by the same polarity remanent flux. To illustrate the fact that the SNLLS based method has a significant advantage over the LLS based method under severe saturation conditions, the compensated results obtained using both these two methods are given in Fig. 6. The result of LLS method is obtained by applying a linear regression on the unsaturated section of the first cycle that appears after the fault occurrence. It can be seen that the accuracy of the LLS method used in this scenario is very low. To improve its accuracy, the unsaturated sections of more than one cycle are required by the method, thus causing a long delay. The ε_{NRMS} is 1.98% in this case.
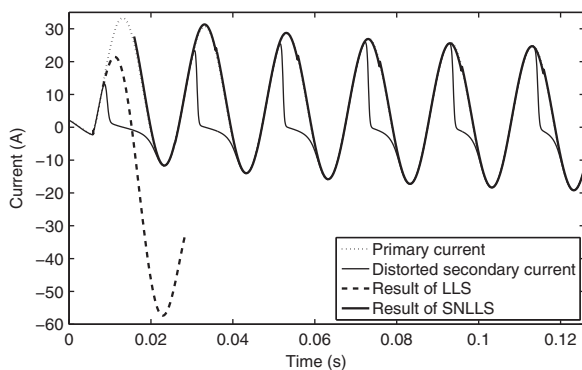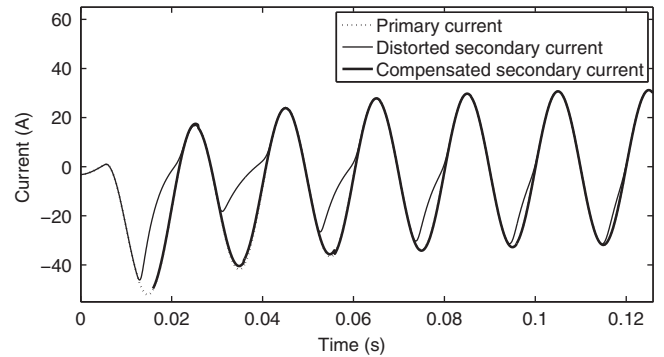

Fig. 6. Compensated result of case 2.

Fig. 7. Compensated result of case 3.

3) *Case 3: 0.5 pf secondary burden scenario*

The secondary burden of a CT, which is the sum of the relay impedance and all the impedance of the secondary circuit loop, is closely related to the saturation level of secondary fault currents. Generally, the larger a secondary burden, the severer the resulting saturation. The shape of the distortion in secondary fault currents is affected by the power factor of the secondary burden. Fig. 7 shows the compensated result of case 3. Due to the 0.5 pf burden, the shape of the saturation curve is different from that of case 1. As shown in the figure, an accurately compensated current can also be obtained within about 10 ms after the fault occurrence. The ε_{NRMS} of this case is 0.43%.

4) *Case 4: large remanent flux and small CT burden scenario*

When a heavy remanent flux is combined with a small CT burden, which is common for digital protection relays, the waveform of the saturation current is close to a sinusoidal waveform. Fig. 8 shows the compensated result of this case. It clearly shows that the compensated secondary current is accurately reconstructed without being affected by the heavy remanent flux. The ε_{NRMS} of this case is 3.92%.

5) *Case 5: AC saturation scenario*

Apart from exponential DC-offset and heavy remanent flux, CT saturation can also be caused by large CT burdens or high symmetrical fault currents. This type of saturation is called AC saturation. In this scenario, a CT saturates in both positive and
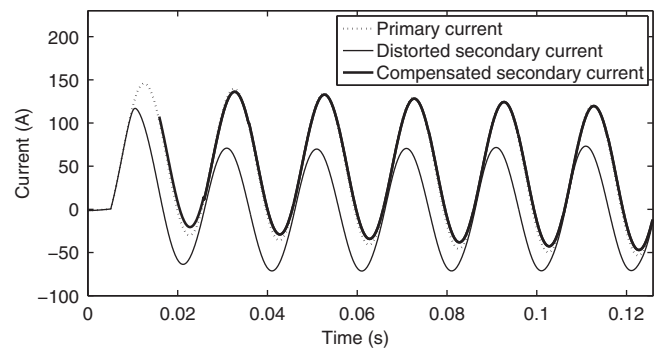

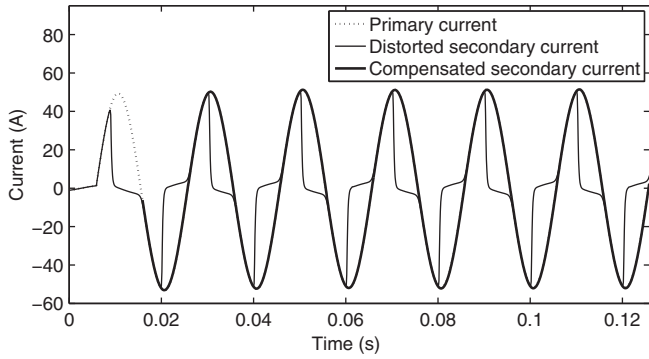**Fig. 8.** Compensated result of case 4.
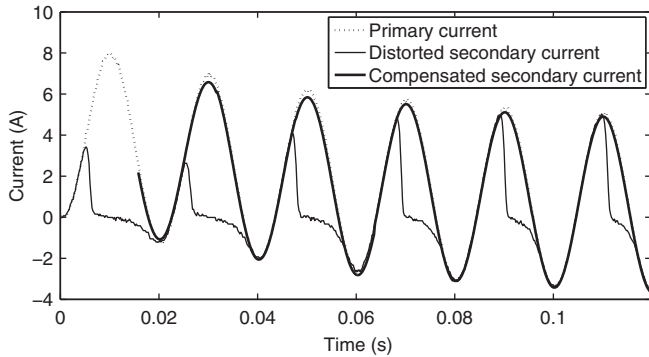
Fig. 9. Compensated result of case 5.

Fig. 10. Compensated result of case 6.

negative polarities of each cycle. The compensation result is shown in Fig. 9. The ε_{NRMS} of this case is 0.2%. This high accuracy is obtained because the absence of exponential DC-offset eliminates the modeling error caused by the first-order Taylor approximation.

4.2. Test cases containing data from a real CT

To evaluate practical performance, the proposed method is applied on the data captured live from a real (miniature) CT. The material of the CT is grain-oriented silicon steel, which is commonly used in the manufacture of line CTs. In total, 84 data sets are processed using the proposed method. These data sets are categorized according to X/R ratio, remanent flux and saturation index. The saturation index, K_1, which indicates the level of saturation, is defined by

$$K_I = \frac{E_{ac}}{E_{sat}} \times 100\%, \tag{16}$$

where E_{ac} is the e.m.f seen at the CT core without any transient component (i.e., in the steady state), and E_{sat} is the e.m.f at which the core flux touches $\pm$ saturation flux in steady state. Since larger noise exists in the live recorded data, the samples of 0.8 cycle are used in the parameter estimation.

Figs. 10 and 11 show the compensated results of two cases, whose configuration are given in Table 2. As shown, the compensation results can be obtained after 0.8 of a cycle from fault occurrence. Their ε_{NRMS} are 4.53% and 3.08%, respectively. The

Table 2
Configurations of test cases 6 and 7.

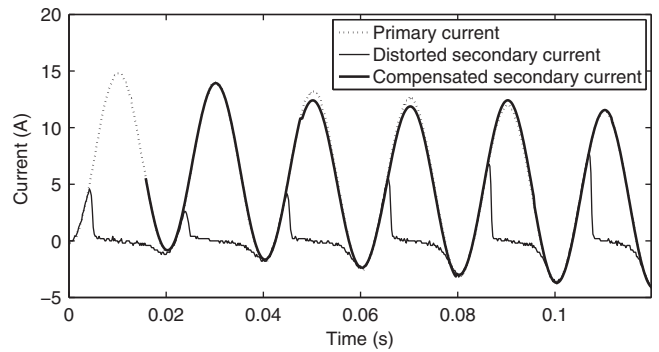|	X/R ratio	Remanent flux	Saturation index
Case 6	20	75%	40
Case 7	50	75%	72

Fig. 11. Compensated result of case 7.

DC-offset decaying speed of case 6 is faster than that of case 7 because of its smaller X/R ratio. Since the first order Taylor series is used to approximate the exponentially decaying DC-offset, a secondary current with a slower decaying DC-offset has a more accurate approximation and a better parameter estimation.

The average ε_{NRMS} of the compensation results of the 84 data sets is 2.16%. And the maximum ε_{NRMS} is 6.54%. It is obtained from the scenario whose configurations are: X/R ratio (20), remanent flux (75%), and saturation factor (18).

5. Hardware implementation and real-time test

5.1. FPGA implementation

The proposed method has been implemented as one of the function modules in the System-on-a-Chip (SoC) based protection relay developed at The University of Liverpool. This relay is designed to take advantage of the flexibility of general microprocessors and performance boosting of paralleled protection modules. The subsystem of the relay, which is relevant to the saturation compensation, is illustrated in Fig. 12. The Nios II microprocessor is in charge of coordinating all the modules in the subsystem. The MLS Based Saturation Detector detects the saturation condition and its polarity using a sliding window of seven samples (this window is in parallel with and shorter than the window used by the proposed method, thus no extra delay is introduced to the compensation outputs by the detector). This detector was developed as a dedicated logic module using Verilog HDL. The SNLLS Based Saturation Compensator has two operation modes, i.e. LLS mode and SNLLS mode, which are used to calculate the parameters $a_1 - a_5$ under nonsaturated and saturated conditions, respectively. The switch between these two modes depends on the results of the detector. Under LLS mode, a_5 is preset to be zero. The calculated parameters are used by the microprocessor to generate compensated currents and the phasors of input currents.

The compensator module is implemented using a specially designed floating point unit (FPU) due to the following reasons:
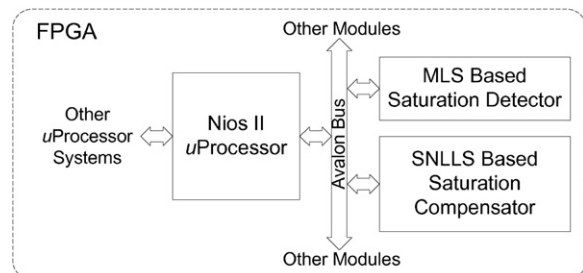

Fig. 12. Block diagram of saturation compensation subsystem.
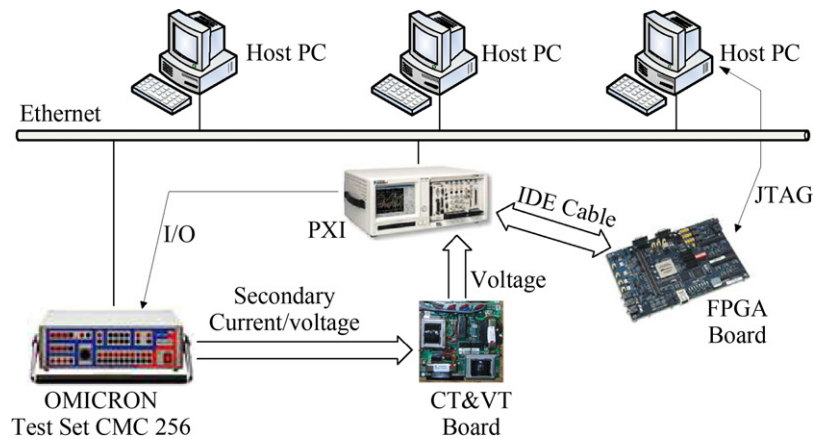
Fig. 13. Hardware structure of the test bench.

(1) a large dynamic range of numbers is required by the SNLLS method, which is difficult to be implemented using fixed-point arithmetic; (2) floating-point elements consume much more FPGA resources than their fixed-point counterparts, therefore element sharing must be applied to reduce resource usage; (3) the complexity of the SNLLS method and the piped lined structures of floating-point elements make the method difficult to be implemented in a fully fixed logic module, thus an FPU is a suitable choice. This FPU has seven paralleled calculation channels and supports some acceleration functions for vector-based calculations. The whole SoC based protection relay is implemented on an Altera DSP Development Board, Stratix II Edition. The performance and resource usage of the compensator module in the FPGA chip are given in Table 3. With an execution frequency of 120 MHz and a 32 points per cycle sampling rate, the calculation can be completed within 0.826 ms. This calculation time is slightly longer than a sampling interval (0.625 ms). However as the consecutive window is employed by the compensator, this calculation time does not cause problems in the real-time implementation. Moreover, the calculation time can be further reduced by using a faster FPGA chip.

5.2. Real-time test

To test the real-time performance of the SoC based protection relay, a real-time protection relay test bench has been established. Its major components and their connections are illustrated in Fig. 13. During the test process, the simulated and live recorded secondary currents are played back by the OMICRON 256 Test Set. These currents are converted to low voltage signals (−5 to +5 V) through a CT board, and then digitized by an IO module in the PXI system, which is an modularized industrial machine running a LabVIEW real-time operating system. The digital samples are transferred to the FPGA board and are processed by the SoC based protection relay implemented inside the FPGA chip of the board. The processed results are sent back to the PXI system and can be observed in real-time through a host PC which displays a remote interface of the PXI system. A screen snapshot of
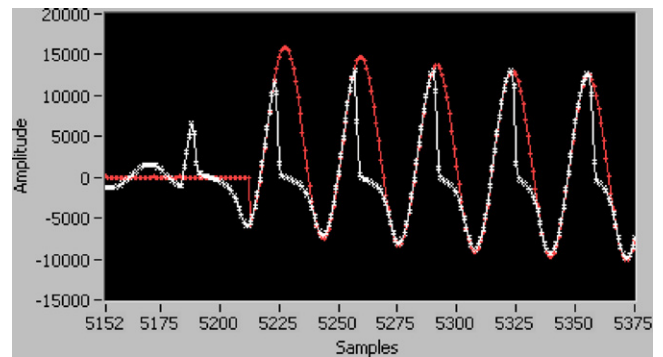

Fig. 14. A snapshot of a compensation test using the test bench.

one compensation test is given in Fig. 14. The white and red lines are a saturated current and its compensated current respectively. Because the communication channels between the PXI system and the FPGA board can only support fixed-point data, the amplitude of these currents is in a fixed-point format. As shown in the figure, an accurate compensated output is available after a delay of 0.8 cycle.

6. Conclusion

This paper presents a promising method for CT saturation compensation. This method obtains accurate parameters faster than the linear regression methods. The fundamental amplitude and phase of the secondary fault current can also be directly obtained from the estimated parameters, which may be used in over-current relays and distance relays to remove the disturbance caused by CT saturation and exponentially decaying DC-offsets. The computational load of the nonlinear regression decreases greatly by applying the SNLLS method. The proposed method has been fully tested with data obtained from both simulation and live recording. It has also been implemented in an FPGA chip and tested in a real-time environment. The test results show the method is capable of providing a reliable input signals to power system protection devices.

Acknowledgements

Table 3
Performance and resource usage of the FPU module.

	Number of usage	Percentage of total resource
Adaptive look-up tables	2359	4.88%
Memory bits	316,027	12.42%
18 × 18 multipliers	36	25%
Maximum frequency (F_{MAX})	120.26 MHz	n/a

References

[1] L.J. Powell, Current transformer burden and saturation, IEEE Transactions on Industry Applications IA-15 (1979) 294–303.

[2] Y. Kang, J. Park, S. Kang, A. Johns, R. Aggarwal, An algorithm for compensating secondary currents of current transformers, IEEE Transactions on Power Delivery 12 (1997) 116–124.

[3] Y.C. Kang, U.J. Lim, S.H. Kang, P.A. Crossley, Compensation of the distortion in the secondary current caused by saturation and remanence in a CT, IEEE Transactions on Power Delivery 19 (2004) 1642–1649.

[4] Z. Lu, J.S. Smith, Q.H. Wu, Morphological lifting scheme for current transformer saturation detection and compensation, IEEE Transactions on Circuits and Systems I: Regular Papers 55 (2008) 3349–3357.

[5] H. Khorashadi-Zadeh, M. Sanaye-Pasand, Correction of saturated current transformers secondary current using ANNs, IEEE Transactions on Power Delivery 21 (2006) 73–79.

[6] K. Erenturk, ANFIS-based compensation algorithm for current transformer saturation effects, IEEE Transactions on Power Delivery 24 (2009) 195–201.

[7] F. Li, Y. Li, R.K. Aggarwal, Combined wavelet transform and regression technique for secondary current compensation of current transformers, IEE Proceedings – Generation, Transmission and Distribution 149 (2002) 497–503.

[8] K. El-Naggar, M. Gilany, A discrete dynamic filter for detecting and compensating ct saturation, Electric Power Systems Research 77 (2007) 527–533.

[9] D. Shi, J. Buse, Q. Wu, L. Jiang, Fast compensation of current transformer saturation, in: Innovative Smart Grid Technologies Conference Europe (ISGT Europe), 2010 IEEE PES, 2010, pp. 1–7, http://dx.doi.org/10.1109/ISGTEUROPE.2010.5638931.

[10] J.R. Lucas, Representation of magnetization curves over a wide region using a non-integer power series, International Journal of Electrical Engineering Education 25 (1988) 335–340.

[11] G. Golub, V. Pereyra, Separable nonlinear least squares: the variable projection method and its applications, Inverse Problem 19 (2003) 1–26.

[12] M.J.D. Powell, Numerical Methods for Nonlinear Algebraic Equations, Gordon and Breach, University of Essex, UK, 1970.

[13] D.W. Marquardt, An algorithm for least-squares estimation of nonlinear parameters, SIAM Journal on Applied Mathematics 11 (1963) 431–441.

[14] R.P. Jajasinghe, P.G. McLaren, Transformer core models based on the Jiles–Atherton algorithm, in: Proc. IEEE WESCANEX 97: Communications, Power and Computing, 1997, pp. 121–125, http://dx.doi.org/10.1109/WESCAN.1997.627124.